International Journal on Magnetic Particle Imaging
Vol 7, No 1, Article ID 2103002, 8 Pages

Infinite Science Publishing

Research Article

Spatial selectivity enhancement in magnetic fluid hyperthermia by magnetic flux confinement

Kulthisa Sajjamark[a,*] · Heinrich Lehr[a] · Rainer Pietig[b] · Niemann Volker[b] · Jochen Franke[a]

[a] Bruker BioSpin MRI GmbH, Ettlingen, Germany
[b] Bruker BioSpin GmbH, Rheinstetten, Germany
*Corresponding author, email: kulthisa.sajjamark@bruker.com

Received 26 October 2020; Accepted 19 February 2021; Published online 29 March 2021

Abstract

Aiming to increase spatial selectivity to enhance the precision in Magnetic Fluid Hyperthermia (MFH) therapy and the spatial resolution in imaging, we propose a strategy to increase the selection field gradient in Magnetic Particle Imaging (MPI). In this study, a solution for an existing MPI system topology was simulated, using an additional soft magnetic material as iron core retrofit at the center of the selection field coil. Due to the core's high magnetic permeability relative to air, the magnetic flux is confined, increasing the selection field gradient. Within this simulation study, the optimal core position is evaluated, whilst its effects on the magnet system are validated. According to our results, this strategy can achieve a 27 % reduction in theranostic field of therapy. We found that this technique increases the magnetic field gradient up to a factor of 1.4 (from 2.5 to 3.4 T/m) in z-direction, without significant loading of the drive field resonance circuit caused by eddy currents in the MPI compatible iron core shielding.

I. Introduction

I.I. Basic theory of MPI

MPI is a new tomographic imaging method which exploits the behavior of superparamagnetic iron-oxide nanoparticles [1]. External alternating magnetic fields are applied to these tracers, while their non-linear response is spatially encoded by a magnetic field gradient [2], featuring a field-free-region. Only unsaturated tracers in this region respond to the magnetic field excitation. The MPI signal is then generated through the rotation of magnetic moment of the particles in response to the excitation [3].

I.II. MPI application in MFH therapy

Alternating magnetic fields can be exploited to rapidly change the magnetic nanoparticles' magnetization. Depending on the used particles and excitation frequencies, the particles' response can be leveraged to either generate signals for imaging or for therapeutic purposes by heat dissipation caused by magnetization losses of the particles. Therefore, MPI is an ideal candidate to assist theranostic hyperthermia due to the similar underlying mechanism in signal and heat generation. Magnetic Fluid Hyperthermia (MFH) has been shown as a cancer treatment strategy by the principles of heat conversion via energy loss in magnetization changes of nanoparticles [4, 5]. This process increases temperature of the tissue locally to the high level. In clinical application,

the temperature in a range of 40°-45° can kill cancer cells, while it causes minimal damage to the surrounding healthy tissue [6]. One challenging approach of brain malign tumor therapy has been recently introduced, in which the brain tissue temperature is increased locally for a few Kelvin only [7]. This leads to the opening of the selective Blood-Brain-Barrier (BBB) allowing for drug-loaded delivery of chemetherapy. A high precision in energy localization is required for this strategy. According to [7], ≤2mm diameter of focus spot by infrared laser illumination was delivered to rodent skull and the localized opening of BBB was then detected.

In order to enable the heating effect, some previous works have demonstrated the use of the scanner's imaging sequences [4, 8] and additional RF-coils [5]. The spatial encoding mechanism in MPI can also be exploited for spatially encoded MFH-therapy. For MPI systems, the magnetic field gradient plays a key role in the encoding mechanism. It was shown in [2], that an increased selection field gradient leads to higher image resolution capabilities. In hyperthermia therapy, an increased spatial selectivity enables more selective energy deposition which can minimize thermal damage in healthy tissue. Similar to [2], the spatial selectivity is dependent on both the therapy tracer properties as well as the selection field gradient slope [4]. Considering the convolution process during MPI signal generation, spatial resolution of MPI as well as spatial localization of hyperthermia is influenced by the magnetization curve of particle response and the full width at half maximum of point-spread-function [2, 4]. By MPI-instrument setting, the size of accessible therapy area is defined by focus field amplitude and gradient of selection field of MPI which are introduced in section II.III. Therefore, the spatial localization of hyperthermia can be controlled and predicted using a MPI system. Both techniques, imaging and therapy, can also be combined into one theranostic system allowing for *in situ* therapy [9, 10]. The increment of temperature in the therapeutic region can be tracked with minimal invasive fiber-optical thermometer or non-invasively by image-guided temperature monitoring proposed in [11]. For an enlarged FOV (Field of View) in imaging or an enlarged FOT (Field of Therapy) in MFH, a homogeneous shift of the Field Free Region (FFR) e.g. using focus fields can be used to superimpose quasi-static magnetic offset fields [1]. In MFH, the offset fields allow for orthogonal shift of the FOT from the magnetic center in any spatial direction.

I.III. Application of ferromagnetic core

Ferromagnetic core placement is a typical way to confine and enhance magnetic fields [12]. According to Biot-Savart law applied to an electromagnetic system [12], the electrical current (I) passing through a coil induces the magnitude of magnetic flux density (**B**). **B** at position

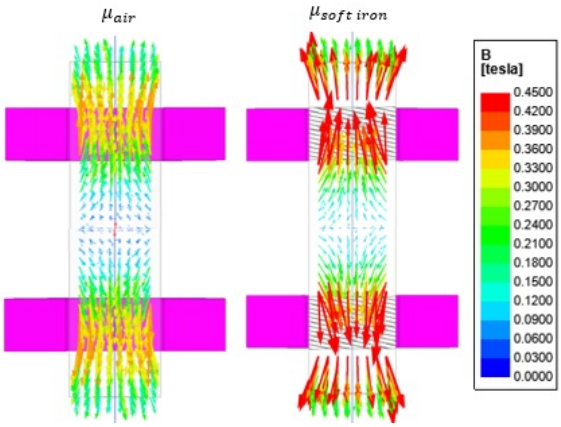

Figure 1: Comparison of simulated magnetic field vectors through Maxwell coils with air- and soft magnetic iron cores.

r with displacement vector $\mathbf{r}\prime$ from wire ($d\mathbf{l}$) can be expressed by

$$\mathbf{B}(r) = \frac{\mu_0}{4\pi} \int_{\text{wire}} \frac{I\, d\mathbf{l} \times \mathbf{r}\prime}{|\mathbf{r}\prime|^3} \tag{1}$$

where $\mathbf{r}\prime = r - l$ and μ_0 is absolute permeablility of air or vacuum.

When a piece of magnetic material is inserted at the coil center, the magnetic flux through the core is confined. The performance of the core can be improved by using a higher magnetic permeability property and an optimal location of the core material [12]. Compared to hard magnetic material, a soft magnetic material has the properties of high permeability and low coercive field [13].

A comparison of magnetic field lines through Maxwell coils with air core and iron core is given in Figure 1. For the coils with soft iron, the magnetic flux is confined and thus, a higher magnetic flux density is enabled. This leads to an increased gradient slope.

II. Material and methods

II.I. Simulation model

A CAD model of a commercially available preclinical MPI system (MPI 25/20 FF, Bruker BioSpin MRI GmbH) with a cylindrical bore and field-free-point (FFP) gradient topology was used to perform the electromagnetic simulations with the software ANSYS Maxwell (ANSYS, Inc., Canonsburg, Pennsylvania, U.S.A).

II.II. Simulation setting

As shown in Figure 2, the 7-channel MPI scanner, consisting of Selection Field (SF) coils, 3-axis Focus Field (FF) coils and 3-axis Drive Field (DF) coils (only DFx coil is

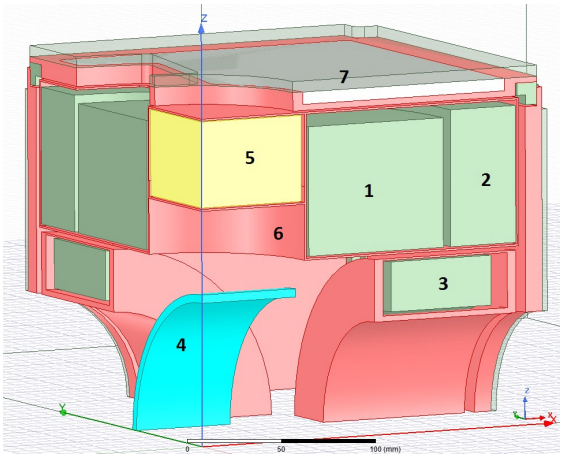

Figure 2: Schematic one-eighth model of the MPI scanner illustrating: 1. SF-coil; 2. FFz-coil; 3. FFx-coil; 4. DFx-coil; 5. Copper-shielded soft iron core at final standard configuration; 6. Copper shields and 7. Soft magnetic Permenorm shield.

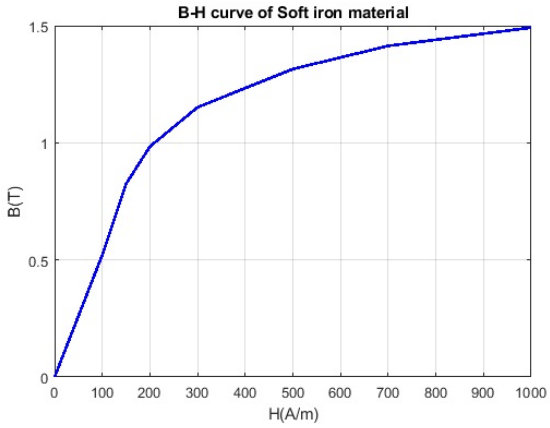

Figure 3: B(H) curve of magnetic induction property of soft iron material applied to the simulation

shown), was augmented by a copper shielded soft magnetic iron core. The static SF coil is used for spatial encoding with an application of field-free-point. DF coil is applied to steer the field-free-region through the field-of-view. FF coil can be used to superimpose magnetic offset field to enlarge field-of-view and -therapy. The copper housing was also applied to cover the SF coils, FFz coils, and iron core in order to limit harmonics effects from DF-excitation and the coupling effect from the respective coils. The magnetic induction B(H) curve shown in Figure 3, corresponding to a soft iron-based core material, was used as soft magnetic material parameter in the simulation. The permeability and non-saturation range of the material can be observed in Figure 3.

Leveraging the coil topology symmetry, the field components of the y-axis were not simulated as they can be predicted by the fields of x-axis. The maximum amplitudes of electrical currents used in this simulation were 500 A_{DC}, 150 A_{DC} and 150 A_{AC} for the SF-coil, FF-coil and DF-coil, respectively. The DF-coil with field direction along the x-axis was simulated with a frequency of 25 kHz which generated the maximum field amplitude of 20 mT. Comparing to DFy and DFz coils, DFx coil locates at the nearest distance to the conductive surface of copper housing, thus, only DFx coil was simulated in this work. The static gradient or SF-field for spatial encoding, which can be adjusted up to maximum values of 1.25/1.25/2.5 T/m for x-, y- and z-axes respectively, was also applied. The detail of coils specification and application can be found in Well's work [8].

II.III. Parameters simulation

The behaviors of the following parameters: SF-gradient slope, SF-gradient linearity error, FF-amplitude, relative FF-homogeneity deviation, FFP offset, DF-induced power loss, and force acting on the core, were considered to evaluate our proposed technique of spatial selectivity enhancement. We also proposed a core optimization method by varying the size and position of the core along z-axis and used the following parameters as the criterions.

1. Slope of field gradient (T/m) which is expressed by:

$$G = \frac{|\mathbf{B}(d_{SF0}) - \mathbf{B}(d_{SF1})|}{d_{SF1}} \tag{2}$$

where the gradient G is calculated by using $\mathbf{B}$ of SF coil at distance along the axis $d_{SF0} = 0$ mm and $d_{SF1} = 10$ mm from the origin coordination, respectively (see Figure 4a).

2. Linearity error L of the field gradient (%) which is determined by:

$$L = 100\left(\frac{|\mathbf{B}(d_{SF0}) - \mathbf{B}(d_{SF2})|}{G\, d_{SF2}} - 1\right) \tag{3}$$

using field gradient slope G and $\mathbf{B}$ of SF coil at distance along the axis $d_{SF0} = 0$ mm and $d_{SF2} = 45$ mm from the origin coordination, respectively (see Figure 4a).

3. Field amplitude of FF coil $\hat{B}_i(d_{FF0})$ (mT) of the specific axis ($i = x$, y, or z) at system's center (see Figure 4b).

4. Relative FF-homogeneity deviations ϵ_{rel} or homogeneity error (%) which can be expressed by:

$$\epsilon_{rel} = 100\left(\frac{|\mathbf{B_i}(d_{FF1})| + |\mathbf{B_i}(d_{FF2})|}{2|\hat{B}_i(d_{FF0})|} - 1\right) \tag{4}$$

where $\hat{B}_i(d_{FF0})$, $\mathbf{B_i}(d_{FF1})$, and $\mathbf{B_i}(d_{FF2})$ of FF coil corresponds to the FF-amplitude and magnitudes of flux density which are plotted against a specific axis

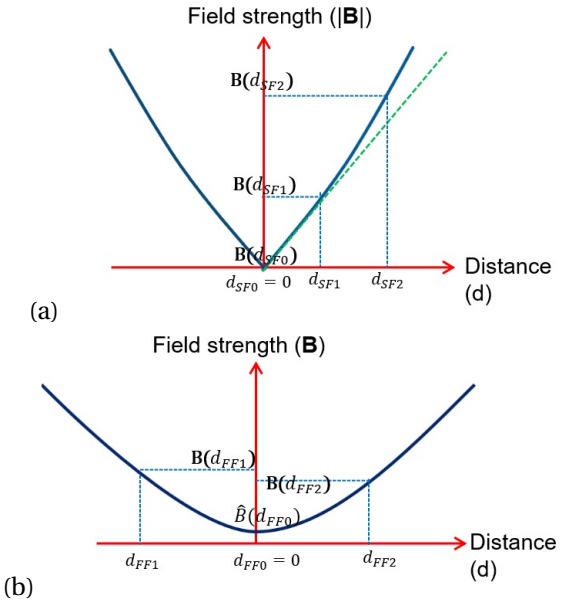

Figure 4: The graphics explain the parameters which were used for the calculations of a) selection field gradient and linearity error and b) focus field's maximum amplitude and relative homogeneity deviations.

($i = x$, y, or z) at distance along the axis $d_{FF0} = 0$ mm, $d_{FF1} = \pm 50$ mm and $d_{FF2} = \pm 50$ mm, respectively (see Figure 4b).

5. Maximum FFP offset or Δi (mm) which can be achieved by FF amplitude ($\hat{B}_i(d_{FF0})$) and the gradient (G_i) at the specific axis ($i = x$, y, or z):

$$\Delta i = \frac{\hat{B}_i(d_{FF0})}{G_i} \tag{5}$$

6. Ohmic or power loss caused by DF-induced eddy-currents in conductive surfaces.
7. Electromagnetic force acting on the inserted core.

Ohmic loss and electromagnetic force were evaluated by the internal workflow of the simulation software.

III. Results and discussion

III.I. Field gradient and core optimization

At first, the iron core was placed at the center of SF-coil aligned with the bottom of SF-coil (see Figure 5b)). The height of the core was set to fit to the available space of coil housing with small gap of 2 mm between the housing and the core. In this setting, the field gradient in z-axis, shown in Figure 6, was boosted up by a factor of 1.6 from 2.5 T/m of the default scanner to 4.2 T/m of the core-inserted scanner. In Figure 6, the resulting gradients were

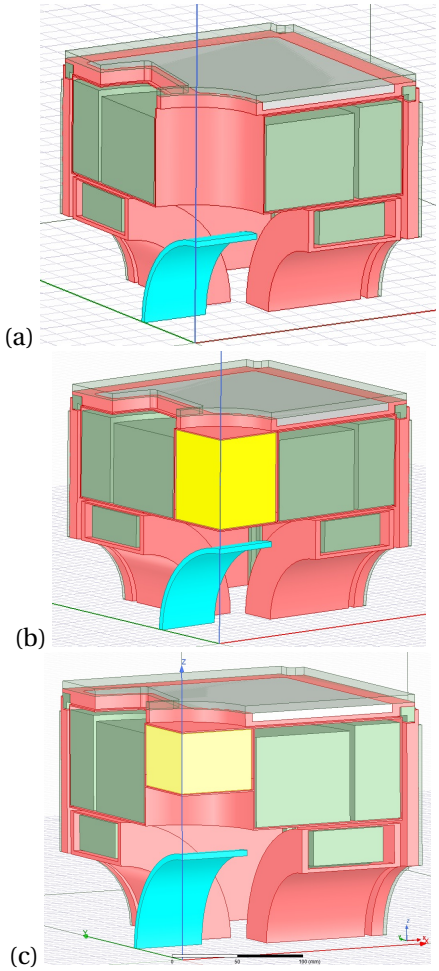

Figure 5: Iron core is added to MPI scanner at two different positions and sizes: a) no core (default scanner topology) b) maximum filling factor and c) at the optimal position.

ploted and compared with their identity lines. Identity line shows ideal gradient which provides the expected gradient value for all distances along the axis. By taking the additional conductive surfaces under the core into account, the DF amplitude was damped by 4 mT with regards to eddy current effect. Considering the energy balance of the system, the DF amplitude is reduced when the input power of DF-coil is constant.

Since the DF amplitude damping reduces the performance of DF-coil and the requirement of additional input power is not desired, the optimization of core localization was proposed. The iron core and its copper shield were shifted away from the DF-coil along z-axis until 20 mT of maximum DF strength was recovered. This position is called henceforward 'optimal position'. At this optimal position, the field gradient calculated by (2), was increased by up to 1.4 times from 2.5 T/m of the default scanner to 3.4 T/m of the scanner with the optimal core position. The gradient linearity error according to (3) was 7.5 % which is slightly increased when compared to

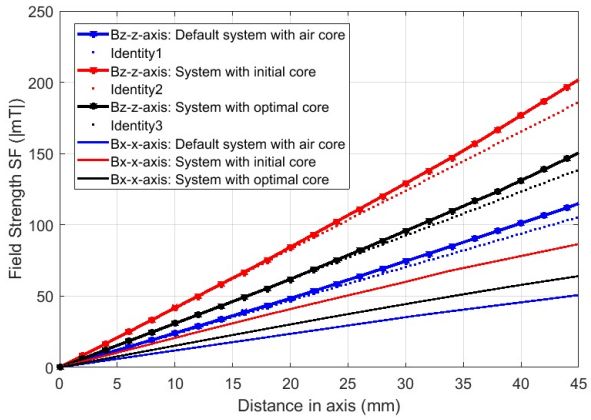

Figure 6: Simulations of SF gradient along x and z-axis and their identity lines are shown for 3 different cases of core modification.

the system without iron core (7.4 %).

The volume of magnetic core relates to the capability of magnetic flux confinement, thus, the decreased volume provides smaller gradient slope in the system. Therefore, the DF amplitude and the gradient of the system need to be balanced in this proposed method.

III.II. Effects on hyperthermia therapy

Considering the process of MPI signal generation, the spatial resolution of the theranostic volume can be determined by the behavior of particle response [2, 4]. For the instrumentation effect, the resolution of heat localization on theranostic region can be indicated by the value of minimum FoT_i which was obtained by using the same calculation as FFP offset in (5):

$$FoT_i = 2\frac{\hat{B}_{RFi}}{G_i} \tag{6}$$

where $\hat{B}_{RFi}$ is the maximum RF-field amplitude of the therapy field and G_i is the gradient slope at the specific axis ($i = x$, y, or z).

In this work, we assume that an additional heating coil was installed to the MPI scanner with a maximum field amplitude of 10 mT in x-direction [10]. Since the topology of the external heating coil was designed to generate only RF field in the x-direction, only the minimal FOT in x-direction was then evaluated. The results showed that our proposed technique provides a reduction in the minimal FoT_x from 16 mm provided by the default system to 11.7 mm by our proposed system which corresponds to a 27 % improvement in the therapy precision. The minimum FOTs for hyperthermia at the maximal gradients of 2.5 T/m for the default and 3.4 T/m for our proposed system are shown in Table 2.

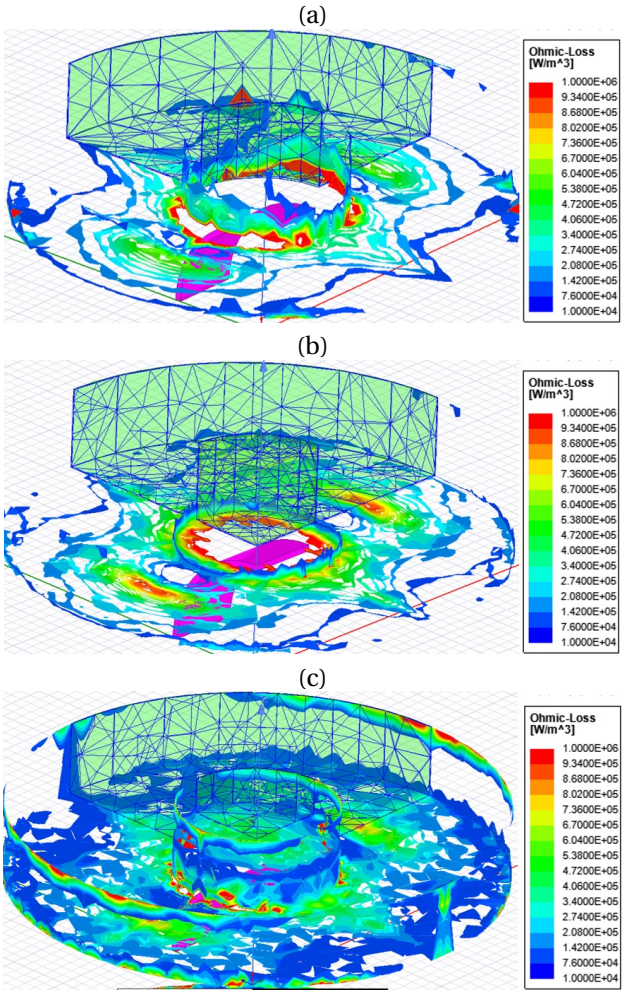

Figure 7: DF-induced ohmic loss distribution on the conductive surface of Z-coils housing shown in 3 cases: a) air core (default scanner) b) core at the initial position and c) core at the optimal position.

III.III. Induced loss distribution

This work proposes an upgradable solution which still preserves our existing system. Copper-shielded magnetic iron core was then added to the system. After we included the magnetic core, the power loss distribution on the conductive material was simulated. Our result showed that most of the losses were induced on the copper component in the housing of Z-coils (SF- and FFz-coils). Since the DF-coil generates an oscillating magnetic field and the direction of the field vector passes directly through the Z-coil housing, high eddy currents were induced into this component. Eddy currents were distributed on the copper screen of the Z-coil as well as the iron core shield. The thickness of the added copper plate under magnetic core was set to 2 mm which is the same value of the entire housing. As this skin effect prevents the 25 kHz excitation to penetrate the 2mm copper screen, there was no eddy current losses found

Table 1: FF amplitude, relative homogenity error and maximum FFP offset capability at maximum gradient in x, y, z directions calculated using (5) for the default magnet system (air core) and the proposed magnet system (iron core at optimal position).

Parameters	**Default**	**Proposed**
max G_x, G_y, G_z (T/m)	1.25/1.25/2.5	1.7/1.7/3.4
$\mathbf{B}_{FF0X}, \mathbf{B}_{FF0Y}, \mathbf{B}_{FF0Z}$ (mT)	18/18/45	18.2/18.2/60
$\epsilon_{xrel}, \epsilon_{yrel}, \epsilon_{zrel}$ (%)	30/30/7	32/32/10
$\Delta X, \Delta Y, \Delta Z$ (mm)	14.4/14.4/18	10.7/10.7/17.5
L_x, L_y, L_z (%)	5.2/5.2/7.4	7.2/7.2/7.5
P_{sum} on coil-Z housing (W)	101.3	90.2

in the magnetic core material. We then investigated the density distribution pattern and magnitude of the DF-induced power loss (P) in the copper surfaces, as shown in Figure 7. The integrated power loss (P_{sum}) over the conductive volume (V) was calculated by using:

$$P_{sum} = \int_{\mathrm{V}} P \, dV. \tag{7}$$

For the default system with air core, the DF-induced loss mostly locates at the edge of copper housing of the Z-coil (see Figure 7a)) with the integrated loss over the shield volume of 101.3 W. After the iron core was placed at the initial position, the ohmic loss got distribution over the coil housing and the iron core shield (see Figure 7b)). In this case, the summed loss value increased around 20 % (118 W) from the default system due to higher induced eddy currents and additional conductive component of iron core shielding. The result in Figure 7b shows that the high magnitude of loss density distributes in the wider area of the copper surface when comparing to Figure 7a.

In comparison between the system with air core (Figure 7a)) and iron core at optimal position (Figure 7c)), the overall DF-induced power loss on copper structures in the system was slightly reduced from 101.3 W to 90.2 W for the system with air core and optimal core, respectively. This reduction of 10 W can be explained by considering the eddy current distribution on the surface. The cross section of eddy current flow path is increased and, thus, the ohmic losses are minimized. Comparing to the default system with air core, the topology of the copper plate in our optimized system was adapted, causing the reduction in eddy current resistance. According to Figure 7, the losses density and magnitude around the shield corner of the optimal-core system (Figure 7c)) were lowered from the air-core system (Figure 7a)) by the additional conductive surfaces introduced together with the iron core.

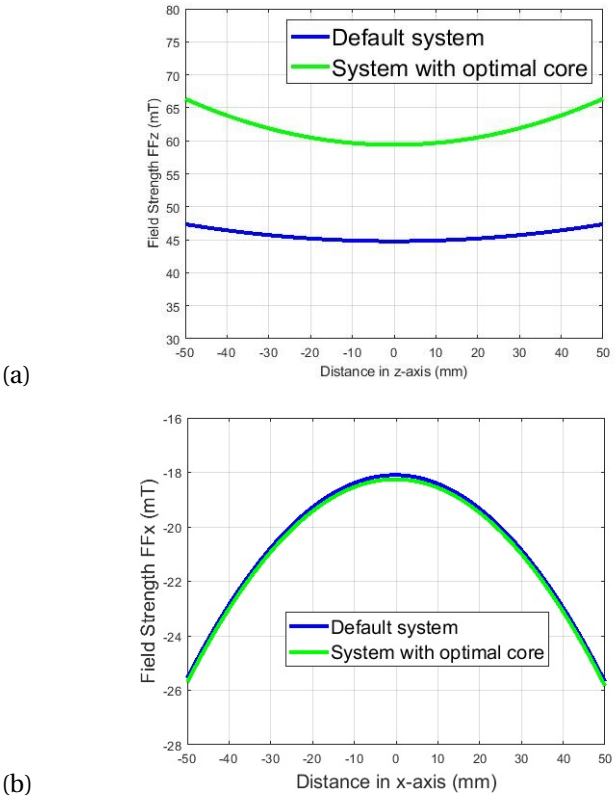

Figure 8: Simulations of FF field along a) the z-axis and b) the x-axis for the default system with air core and proposed system with optimal core were compared.

III.IV. Effects on focus field and field of view

According to our results, the maximum FF-amplitude was increased in z-direction. Comparing the maximum FFz amplitude of 45 mT for the default system and 60 mT for the system with the optimal core position (see Figure 8a), the maximum FFP offsets in z-direction by (5) are 18 and 17.5 mm while FFz homogeneity error using (4) are 7 % and 10 %, respectively. The field amplitudes and the homogeneity of the FFx and FFy were not affected significantly by the iron core, as expected (see results in Table 1). However, regarding to (5), the maximal FFP offsets in x- and y-direction were affected by the incresed gradient slope from 14.4 mm for the default scanner with air core to 10.7 mm for the proposed scanner with iron core. The resulting maximum FFP offset causes 25 % reduction in FOV in x- and y-direction which limits the accessible FOT. For the FOV in z-direction, no significant change is induced by our proposed system. The maximal FFP offset by the focus field at the maximal gradients of 2.5 T/m for the default and 3.4 T/m for our proposed system are shown in Table 1.

Table 2: Minimum FOTs for hyperthermia and estimated imaging resolution [2] in x, y, z directions for the default (air core) and proposed (core at optimal position) magnet systems.

Parameters	**Default**	**Proposed**
max G_x, G_y, G_z (T/m)	1.25/1.25/2.5	1.7/1.7/3.4
min accessible FoT (mm) at $\hat{B}_{RF}$ 10mT	16/0/0	11.7/0/0
max accessible FoT (mm) at $\hat{B}_{RF}$ 10mT	28.8/28.8/36	21.4/21.4/35
Spatial imaging resolution estimation (mm) [2]	2/2/1	1.5/1.5/0.75

III.V. Effects on spatial resolution of MPI imaging

In addition to the benefit of therapeutic precision, this work also offered the improvement of resolution in theranostic imaging. With e.g. a nanoparticle size of 30 nm, the native resolution during imaging was estimated by the simulation result in Rahmer's work [2] to increase by 25 % by our proposed system compared to the default system caused by an increased gradient amplitude [2] (see Table 2).

III.VI. Selection and focus coils-induced force on core

For the force simulation, the force is calculated by using the principle of virtual work. The virtual work is formed by the flux density (**B**) and the applied magnetic field (**H**) over the volume (V) expressed by

$$W = \int_{\mathrm{V}} \left(\int_{\text{BH-loop}} \mathbf{B}\, d\mathbf{H} \right) dV. \tag{8}$$

The resulting virtual force on the core is obtained by the change of virtual work (W) over the distance of field source in relation to the core region where the force acts (s),

$$F_{core} = \frac{dW(s)}{ds}. \tag{9}$$

The simulation showed that the force was mostly generated by the SF-coil and FFz-coil which are located in the MPI magnet system with an alignment in z-axis, same as the iron core. According to the virtual force simulation, a SF-coil generates 450 N, a FFz-coil generates ±100 N and the force by FFx- and FFy-coil is negligible.

IV. Conclusion

This research presents a simulation study of a MPI scanner modification to enhance the spatial selectivity of localized MFH and imaging by including an additional soft magnetic iron core. The increased gradient in x-direction, with a factor of 1.4, provides almost 27 % increase in precision of targeting in hyperthermia with the presence of an external RF-coil (see calculation in (6)). Apart from hardware adaptation, the spatial resolution of theranostic FOT can be determined by particle optimization. An increased gradient from 2.5 to 3.4 T/m can also lead to 25 % improvement of native image resolution estimation in MPI imaging, when considering particle sizes of 30 nm [2]. According to the simulation of DF-induced power loss, the final configuration of the iron core and its housing, which were provided by our proposed optimization method, causes no additional loss when compared with the default system with air core. However, the resulting maximum achievable FOV was reduced in x- and y-direction by the increase of the resulting gradient. This must be compensated by an increased current density in FFx and FFy coils. Regarding to force simulation, the proper mechanical fixation of the core in the scanner need to be designed in order to support the acting force of more than 500 N in worst case.

Inserting magnetic material is an affordable, cost-effective, and low-effortful method to increase the SF gradient without the need for additional power consumption. Furthermore, this technique allows for an easy upgrade of existing magnet systems. The core localization significantly influences the performance of the magnet system in terms of selection and focus fields mainly in z-axis. In this study, the core position was optimized to find a functional compromise between the gain of the increased gradient slope and DF-induced field loss. In future, practical experiments will be performed to validate the therapeutic selectivity enhancement using the proposed insertion of soft magnetic material. Moreover, the effect on time response of the different coils in alternating-current devices must also be evaluated as the changing magnetic field causes frequency-dependent energy loss.

Acknowledgments

The work is a part of Functional Magneto-Therapy project which is funded by the German Federal Ministry of Education and Research (BMBF, grant number 13GW0230C). We would like to express the special thanks to our colleage, Jorge Chacon Caldera, who helped and supported us during the research and writing process.

References

[1] B. Gleich and J. Weizenecker. Tomographic imaging using the nonlinear response of magnetic particles. *Nature*, 435(7046):1214–1217, 2005, doi:10.1038/nature03808.

[2] J. Rahmer, J. Weizenecker, B. Gleich, and J. Borgert. Signal encoding in magnetic particle imaging: properties of the system function. *BMC Medical Imaging*, 9:4, 2009, doi:10.1186/1471-2342-9-4.

[3] J. Weizenecker, J. Borgert, and B. Gleich. A simulation study on the resolution and sensitivity of magnetic particle imaging. *Physics in Medicine and Biology*, 52(21):6363–6374, 2007, doi:10.1088/0031-9155/52/21/001.

[4] Z. W. Tay, P. Chandrasekharan, A. Chiu-Lam, D. W. Hensley, R. Dhavalikar, X. Y. Zhou, E. Y. Yu, P. W. Goodwill, B. Zheng, C. Rinaldi, and S. M. Conolly. Magnetic Particle Imaging-Guided Heating in Vivo Using Gradient Fields for Arbitrary Localization of Magnetic Hyperthermia Therapy. *ACS Nano*, 12(4):3699–3713, 2018, doi:10.1021/acsnano.8b00893.

[5] K. Murase, M. Aoki, N. Banura, K. Nishimoto, A. Mimura, T. Kuboyabu, and I. Yabata. Usefulness of Magnetic Particle Imaging for Predicting the Therapeutic Effect of Magnetic Hyperthermia. *Open Journal of Medical Imaging*, 05(02):85–99, 2015, doi:10.4236/ojmi.2015.52013.

[6] M. Roesch and B. Mueller-Huebenthal. Review: The Role of Hyperthermia in Treating Pancreatic Tumors. *Indian Journal of Surgical Oncology*, 6(1):75–81, 2015, doi:10.1007/s13193-014-0316-5.

[7] P. Schlett, S. Mottaghi, O. Buchholz, and U. G. Hofmann. First Steps towards Localized Opening of the Blood-Brain-Barrier by IR Laser Illumination Through the Rodent Skull. *Current Directions in Biomedical Engineering*, 5(1):211–214, 2019, doi:10.1515/cdbme-2019-0054.

[8] J. Wells, S. Twamley, A. Sekar, A. Ludwig, H. Paysen, O. Kosch, and F. Wiekhorst. Lissajous scanning magnetic particle imaging as a multifunctional platform for magnetic hyperthermia therapy. *Nanoscale*, 12(35):18342–18355, 2020, doi:10.1039/D0NR00604A.

[9] A. Malhotra, A. von Gladiss, A. Behrends, T. Friedrich, A. Neumann, T. M. Buzug, and K. Lüdtke-Buzug. Tracking the Growth of Superparamagnetic Nanoparticles with an In-Situ Magnetic Particle Spectrometer (INSPECT). *Scientific Reports*, 9(1):10538, 2019, doi:10.1038/s41598-019-46882-6.

[10] A. Behrends, H. Wei, T. Friedrich, A. Neumann, and T. M. Buzug, A self-compensating coil setup for combined magnetic particle imaging and magnetic fluid hyperthermia, in *International Workshop on Magnetic Particle Imaging*, 2019.

[11] C. Stehning, B. Gleich, and J. Rahmer. Simultaneous magnetic particle imaging (MPI) and temperature mapping using multicolor MPI. *International Journal on Magnetic Particle Imaging*, 2(2), 2016, doi:10.18416/IJMPI.2016.1612001.

[12] A. Moses, P. Anderson, and K. Jenkins, Electrical Steels: Fundamentals and Basic Concepts. Institution of Engineering and Technology, 2019, doi:1785619705.

[13] K. M. Krishnan, Fundamentals and Applications of Magnetic Materials. Oxford University Press, 2016, ISBN: 9780199570447.

